We are IntechOpen,
the world's leading publisher of
Open Access books
Built by scientists, for scientists

6,900
Open access books available

185,000
International authors and editors

200M
Downloads

Our authors are among the

154
Countries delivered to

TOP 1%
most cited scientists

12.2%
Contributors from top 500 universities

BOOK CITATION INDEX
CLARIVATE ANALYTICS
INDEXED

WEB OF SCIENCE™

Selection of our books indexed in the Book Citation Index
in Web of Science™ Core Collection (BKCI)

Interested in publishing with us?
Contact book.department@intechopen.com

Numbers displayed above are based on latest data collected.
For more information visit www.intechopen.com

Impedimetric Immunosensor for Pesticide Detection

Saloua Helali

Additional information is available at the end of the chapter

1. Introduction

Pollution of surface water by chemicals can disturb aquatic eco-systems and cause loss of habitats and reduce biodiversity. Pollutants may accumulate in the food chain, and harm predators consuming contaminated fish. Humans are exposed to pollutants through the aquatic environment by fish or seafood consumption, drinking water and possibly recreational activities. Pollutants may be found in the environment many years after being banned; some may be transported over long distances and can be found in remote areas. Pollutants may be released in the environment from various sources, e.g., agriculture, industry, incineration, as products or as unintended by-products, they may have been released in the past or continue to be released from consumer products used in everyday life.

Recently, the European Commission adopted a proposal for a new Directive to protect surface water from pollution by chemicals (COM(2006)397 final) [1]. The proposed Directive will set limits on concentrations in surface waters of 41 dangerous chemical substances including 33 priority substances and 8 other pollutants that pose a particular risk to animal and plant life in the aquatic environment and to human health. Pesticides are important pollutants and are hazardous to human health and life. During the past 50 years, pesticides have been used in increasing amounts throughout the word. Among pesticides, atrazine (2-chloro-4-ethylamino-6-isopropylamino-1,3,5-triazine) is the most extensively applied herbicide to control broad-leaf plants and grassy weeds, because of its high relative mobility in the soil in the world [2-7]. Atrazine is a putative endocrine disruptor and may cause serious health risks even at very low levels (parts-per-billion concentration). At high concentrations (100 μgl^{-1}), it causes dramatic effects on the photosynthesis, growth, chlorophyll content and biomass of most aquatic producers [5]. Long-term exposure of humans and animals to atrazine at low concentrations may induce subacute injury and potential hazards to the body. Although studies on the toxicity of atrazine on humans have not been completely con-

clusive, atrazine exposure in rodent models has identified reproductive and developmental abnormalities. The maximum level for atrazine contamination is 3.0 ppb in drinking water, as established by the US Environmental Protection Agency [8].

The standard procedure for pesticide determination in water is extraction (liquid-liquid, liquid-solid), followed by chromatographical separation and specific detection (UV-visible spectroscopy)[9]. Such techniques are reliable and currently used but they require purification of samples prior to assay, thus limiting the number of samples that can be analyzed [10]. In addition, these conventional approaches are expensive, time consuming, frequently generate considerable waste, and require highly trained personnel. Moreover, conventional environmental monitoring typically involves several steps such as sampling, sample handling, and sample transportation to a specialized laboratory that prevents real-time on-site detection of the sample toxicity. These disadvantages of traditional analytical methods have paved the way for the development of atrazine biosensors as simple, fast, sensitive, selective, cost-effective, real-time, on-site, and field portable monitoring technologies with negligible waste generation[11-13].

Due to the highly sensitive and selective nature of the recognition between antigen (Ag) and antibody (Ab), immunoassays are very useful in widespread applications such as medical detection, processing quality control, and environmental monitoring. Traditional methods used in immunoassays involve radioimmunoassay (RIA) and enzyme-linked immunosorbent assay (ELISA). Although they are sensitive, RIA exposes laboratory workers to a significant safety hazard, and ELISA is tedious and time-consuming. New techniques, such as electrochemistry, chemiluminescence, piezoelectricity and surface Plasmon resonance have attracted extensive interest in immunoassays due to their simple and specific characteristics. Among these techniques, electrochemical immunoassay has received much attention for its high sensitivity and low cost. As most antibodies and antigens are electrochemically inert, the label-free technique of electrochemical impedance spectroscopy (EIS) is developed to provide a direct detection of immunospecies by measuring the change of impedance. In addition to its convenience, EIS provides a nondestructive means for the characterization of the electrical properties in biological interfaces [14-15].

2. Biosensors overview

A biosensor can be described as a transducer that incorporates a biological recognition component as the key functional element. It consists of three main components as illustrated in Fig. 1: the biorecognition element, the transducer and the signal display or readout [16]. The interaction of the analyte with the biorecognition element is converted to a measurable signal by the transduction system. The signal is then converted into a readout or display. Analytical immunosensors are a subset of biosensors which utilize either antigen or antibody as the biospecific sensing element.
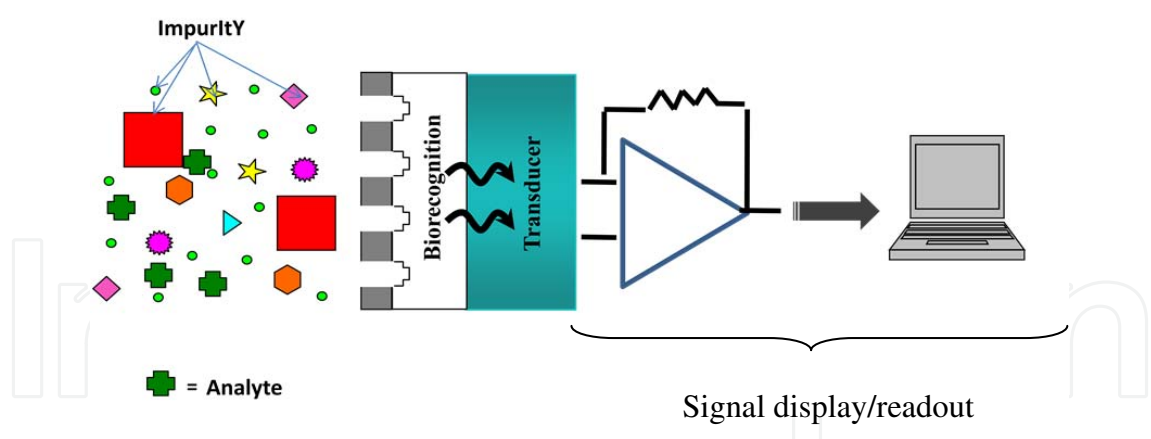
Figure 1. Composition of a biosensors

When antibodies or antibody fragments are used as molecular recognition element for specific analytes (antigens) to form a stable complex, the device is called immunosensor [17].

Many kinds of nanomaterials, including metal nanoparticles (gold, magnetic beads), polymer (polypyrrole), and carbon nanotubes (CNTs) have been widely used in immunosensor (Fig.2). The common characteristics of these nanomaterial in immunosensor are providing signal amplifications comparing to the traditional metal ion labels, enzyme labels and redox probe labels[18].
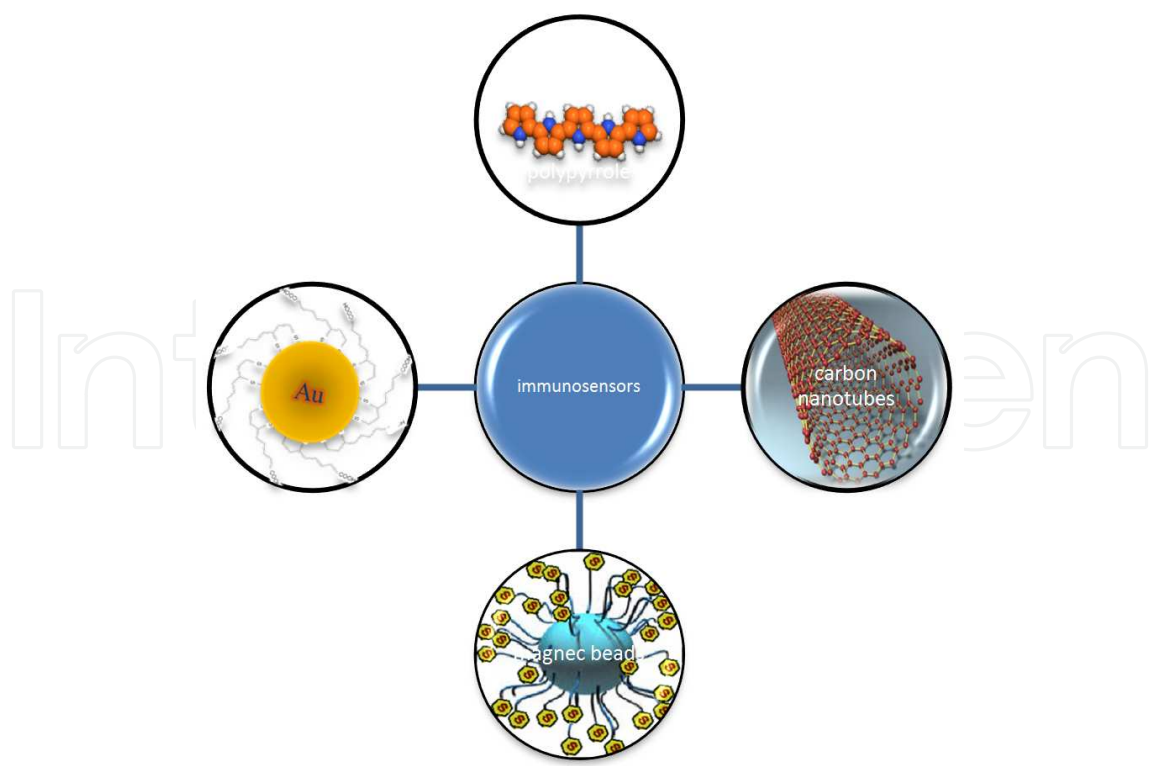
Figure 2. Nanomaterial used in immunosensor

Electrodes are commonly made of inert metals such as platinium, gold or carbon, either in the of graphite, glassy carbon as a solid or as a paste. These electrodes are commonly used to detect chemical compounds produced or consumed by binding. Therefore, for the construction of impedimetric immunosensors are needed.

2.1. Biosensors for monitoring pesticides

The first synthetic pesticides became available during the 1940s, generating large benefits in increased food production. Each year an estimated 2.5 million tons of pesticides are applied to agricultural crops worldwide. Pesticides can be classified into three different groups: insecticides, herbicides and fungicides. Insecticides are usually organophosphorous compounds (e.g. parathion), organochlorine compounds (e.g. DDT) or carbamates (e.g. carbofuran). Fungicides are either sulphur, copper or organic based compounds, while herbicides can be either organic or inorganic compounds. Pesticides can be applied as dust or granules, as a vapour or more commonly applied as, or in the presence of a liquid (water or oil usually). Pesticides, depending on their water solubility can either remain in the soil to be broken down by the action of certain organisms [19], or washed off, eventually washing into rivers and sometimes water supplies. The persistency of pesticides and of their degradation products in the geosphere causes environmental problems. The transfer of pesticides from treated soil to surface and ground water leads to contamination of drinking water resources and to subsequent intake of pesticides by man.

Pesticides can be carcinogenic, citogenic, they can produce bone marrow diseases, infertility, nerve disorders and immunological and respiratory diseases [20]. For these reasons, there is a growing demand for fast and reliable pesticide monitoring in agriculture and food production. Recently there has been a large increase in the number of publications concerning biosensors for monitoring pesticides.

A biosensor for the detection of carbamate insecticides was based on the action of enzymes, acetylcholinesterase [21]. Carbamate pesticides inhibited acetylcholinesterase and the decrease in the enzyme activity was used to determine these pesticides. Acetylcholinesterase was immobilized on silica gel by covalent binding. pH and conductivity electrodes were used to detect the ionic change of the sample solution due to hydrolysis of acetylcholine. The biosensors were used to analyze carbaryl in water.

The optical transducer of CdTe semiconductor quantum dots (QDs) has been integrated with acetylcholinesterase enzyme (AChE) by the layer-by-layer assembly technique, resulting in a highly sensitive biosensor for detection of organophosphorus pesticides (OPs) in vegetables and fruits based on enzyme inhibition mechanism[22]. The detection limits of the proposed biosensors are as low as 1.05×10^{-11} M for paraoxon and 4.47×10^{-12} M for parathion.

An amperometric biosensor which used the enzyme an acetylthiocholine (ATCh) has been used for detection and quantification of three organophosphorus pesticides – paraoxon ethyl, monocrotophos and dichlorvos. The inhibition curves for each pesticide was plotted and the linear intervals were determined along with the corresponding equations and detection

limits – 0.87× 10^{-11} M for paraoxon, 1.08× 10^{-11} M for monocrotophos and 1.22 × 10^{-10} M for dichlorvos [23].

Clemens Steegborn and Petr Skliidalt described a piezoelectric immunosensor for determination of the herbicide atrazine. The Interaction of the anti-atrazine monoclonal antibody (MAb, clone D6F3) with the immobilized atrazine was characterized using both crude ascetic fluid and Protein A-purified MAb preparates. As expected, the higher dilutions of MAb provided improved sensitivity for the analyte. For the 1000X diluted ascetic fluid, 0.1 and 1 µg/l atrazine caused 5 and 30% decreases of the relative binding of MAb, respectively [24].

3. Electrochemical impedance spectroscopy (EIS)

Impedimetric immunosensors have recently received particular attention since they possess a number of attractive characteristics associated with the use of electrochemical transducers, namely, low cost of electrode mass production, cost effective instrumentation, the ability to be miniaturized and to be integrated into multi-array or microprocessor-controlled diagnostic tools, remote control of implanted sensors, etc. Indeed, due to the above-mentioned characteristics, electrochemical impedance spectroscopy (EIS)-based sensors are considered as promising candidates for use at on-site applications [25,26].

3.1. Fundamentals [27-29]

Electrochemical Impedance Spectroscopy (EIS) is the method in which the impedance of an electrochemical system is studied as a function of the frequency of an applied a.c. wave.

When the system is perturbed (by applied a.c. voltage) it relaxes to a new steady state. The time taken for this relaxation is known as the time constant, τ, and given by:

$$\tau = RC$$

where R is the resistance and C the capacitance of the system. The analysis of this relaxation process would provide information about the system. The ratio of the response to the perturbation is the transfer function. When the applied perturbation is an a.c. potential and the response an ac. current, the transfer function is the impedance. To simplify calculations further, the perturbation and response are transformed from a function of time into the frequency domain via a Laplace transformation. The applied potential is given by

$$\underline{E} = E_0 \exp(j\omega t) \tag{1}$$

where E0 is the amplitude of the signal and $\omega = 2\pi f$ is the radial frequency and f is frequency

The output current of the system is also a sinusoidal, is shifted in phase (φ) and has a different amplitude, I_0 and it is given by,

$$\underline{I} = I_0 \exp\left(j\omega t + \varphi\right) \qquad (2)$$

According to Ohm's law, impedance (Z) of the circuit at any frequency (ω) can be represented by:

$$\underline{Z} = \frac{\underline{E}}{\underline{I}} = \left(\frac{E_0}{I_0}\right)\exp\left(-j\varphi\right) = Z_0 \exp\left(-j\varphi\right) \qquad (3)$$

The impedance is therefore expressed in terms of a magnitude, Z_o, and a phase shift, φ. It is possible to express the impedance as:

$$\underline{Z} = Z_0 \cos\left(\varphi\right) - jZ_0 \sin(\varphi) = Z^{'} - jZ^{''} \qquad (4)$$

The expression for $\underline{Z}$ is composed of a real and an imaginary part.

Usually a low a.c. voltage of about 10 mV is applied to keep the system linear.

The most popular formats for evaluating electrochemical impedance data are the Nyquist and Bode plots. In the former format, the imaginary impedance component ($Z^{''}$) is plotted against the real impedance component ($Z^{'}$) at each excitation frequency, whereas in the latter format, both the logarithm of the absolute impedance, |Z| and the phase shift, φ, are plotted against the logarithm of the excitation frequency.

3.2. Equivalent circuit

Interpretation of EIS measurements is usually done by fitting the impedance data to an equivalent electrical circuit which is representative of the physical processes taking place in the system under investigation. In fact, one of advantages of EIS is that impedance functions frequently display many of the features exhibited by passive electrical circuit.

The most important elements that can be used in equivalent circuits are summarized in table 1. The resistor, R, represents the resistor that charge carriers encounter in a specific process or material. The capacitor, C, represents the accumulation of charged species. The inductance, L, is used to represent the deposition of surface layers such as the passive layer. The Warburg element, W, is used to model linear semi-infinite diffusion which occurs when the diffusion layer has infinite thickness. The constant phase element, CPE, is a general element which can represent a variety of elements such as inductance (n=-1), resistance (n=0), Warburg (n=0.5), capacitance (n=1).

| Element	Symbol	Impedance expression
Resistance	R	R
Capacitance	C	$1/(jc\omega)$
Inductance	L	$jl\omega$
Warburg	W	$1/[Y(j\omega)^{1/2}]$
CPE	Q	$1/[Y(j\omega)^n]$

Table 1. Electrical impedance elements

Capacitive immunosensors exploit the change in dielectric properties and/or thickness of the dielectric layer at the electrolyte–electrode interfaces, due to the antibody–antigen interaction, for monitoring this process. An electrolytic capacitor (working electrode/ electrolyte) allows the detection of an analyte specific to the receptor that has been immobilized on the surface of the working electrode. Ideally, this configuration resembles a capacitor in its ability to store charge and thus, the electric capacitance between the working electrode and the electrolyte is given by equation 5:

$$C = \frac{\epsilon_0 \epsilon S}{d}$$

(5)

Where ε, is the dielectric constant of the medium between the plates, εo, is the permittivity of free space (8.85419pF/m), S, is the surface area of the plates, and, d, is the thickness of the insulating layer (m).

A decrease of the total capacitance, due to the increase of the distance between the plates is thus expected upon the binding of the analyte to its specific receptor.
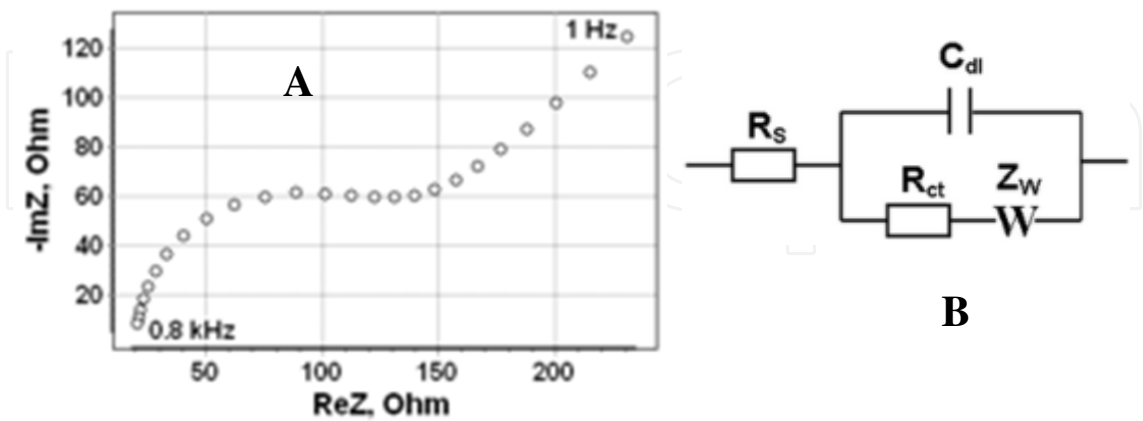
Figure 3. Nyquist plot arising from a Randles circuit showing in the side panel

While no equivalent model can be guaranteed to be unique, simulation of the recorded impedimetric data to an equivalent electric circuit is a common strategy for understanding the

physical origin of the observed response. The simplest, and in fact the most frequently used equivalent circuit for modelling of EIS experimental data is the so called Randles circuit (Fig. 3.B), which comprises the uncompensated resistance of the electrolyte (Rs), in series with the capacitance of the dielectric layer (Cdl) and the charge-transfer resistance (Rct), if a redox probe is present in the electrochemical cell. The latter two components are connected in parallel. An additional component, connected in series with Rct, the Warburg impedance (Zw) accounts for the diffusion of ions from bulk electrolyte to the electrode interface. A typical shape of the impedance spectrum of this circuit presented in a Nyquist plot (Fig. 3.A) includes a semicircle region lying on the real axis followed by a straight line. The linear part ($\phi=\pi/4$), observed at the low frequency range, implies a mass-transfer limited process, whereas the semicircle portion, observed at high frequency range, implies a charge-transfer limited process.

4. Bioreceptors

The sensitivity of immunosensor is strongly dependant on the amount of immobilized antibodies and their remaining antigen binding properties. A variety of immobilization methods for proteins has been reported in the literature [30]. The choice of the optimal immobilisation method not only depends on the surface linking layer and its specific functional end groups but also on the free functional groups in the antibodies or their respective fragments. Numerous bi-functional cross linking reagents have been developed using reactive chemical groups such as succinimide esters and aldehyde groups. These linkage strategies selectively form covalent bonds with the lysine residues randomly present in the antibodies, giving rise to a random orientation of the receptor molecules immobilized on the sensor surface.

4.1. Mixed biotinylated self-assembled monolayer

Self-assembled monolayers consisting of long alkyl-thiols chains on gold have been shown to be stable in air, water and organic solvents at room temperature [31]. On the other hand, the biotin/neutravidin couple has a quite high binding affinity and can act as a bridge to anchor bioreceptor species. Therefore, a stable self-assembling system combined with a biotin/neutravidin couple has potential application for construction of biosensors. In this study, a mixed monolayer is chosen, which is composed of 1,2 dipalmitoyl-sn-glycero-3-phosphoethanolamine N-(biotinyl) (biotinyl-PE) and 16-mercaptohexadecanoic acid (MHDA). It possess a thiol group allowing its immobilization on gold surfaces, and an hydrophilic terminal carboxyl group. The final stability of the mixed SAM layer is obtained through hydrophobic interaction between long alkyl (C16) chains. Fig.4 shows the assembly of the mixed SAM.

After the mixed MHDA/biotinyl-PE self-assembled monolayer was formed on gold electrode and in order to reduce non-specific adsorption, an anti-goat IgG was used to block the free space between biotinyl-PE molecules in the mixed SAM. Then, neutravidin was bound on the biotinyl-PE. Like streptavidin, neutravidin can bind four biotinyl groups, so it can act as a cross-linking agent between different molecular layers. Neutravidin is used as an alter-

native to streptavidin as it is carbohydrate free and has a neutral isoelectric point, which provides exceptionally low nonspecific binding properties. In the following step, biotinyl-Fab fragment K47 antibody was anchored onto neutravidin to allow the specific affinity immobilization of atrazine.
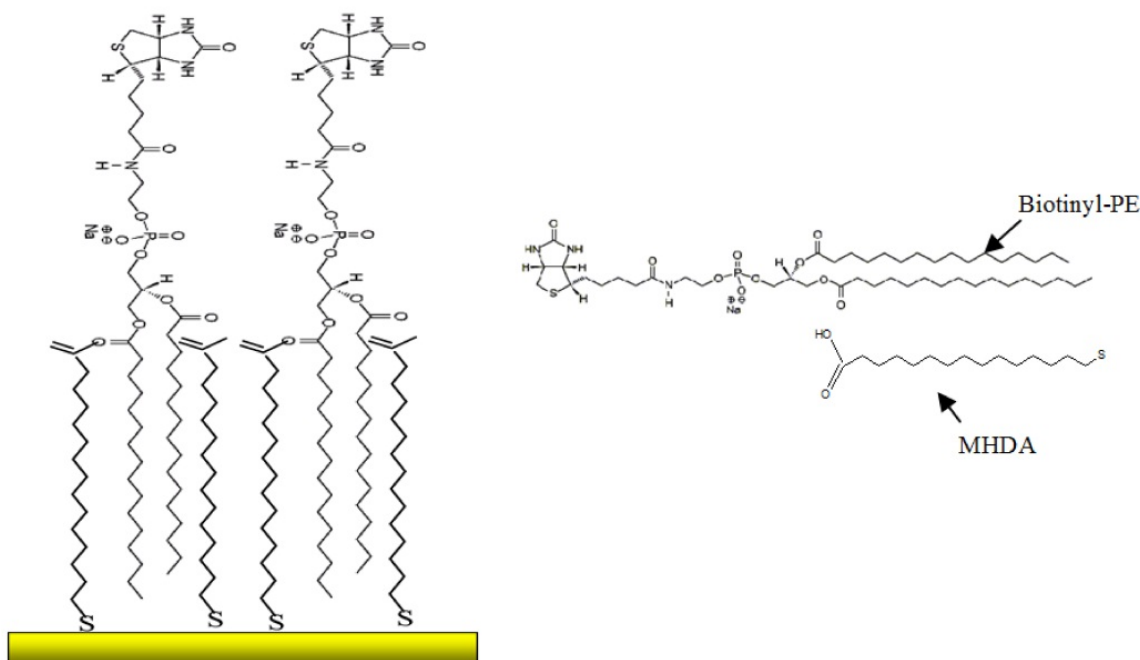
Figure 4. Schematic showing the assembly of a mixed self-assembled monolayer.

4.1.1. Electrochemical characteristics of mixed self-assembled monolayer [32]

The properties of mixed monolayer were characterized by cyclic voltammetry and impedance spectroscopy techniques.

Complex impedance plots of bare electrode (a) and mixed self-assembled monolayers (b) are shown in Fig. 6.A. The impedance spectra of bare gold electrode fit the theoretical profile and include a semi-circle region in the frequency range from 0.5 to 1×10^5 Hz. For the mixed self-assembled monolayers deposited on the gold electrode, the impedance spectra include a semi-circle region observed at high frequencies, corresponding to a change in the SAM structure, followed by a linear region characteristic of lower frequencies attributed to diffusion phenomenon. The respective compressed semi-circle diameters correspond to the membrane resistance at the electrode surface, and increase on the addition of self-assembled monolayers on the electrode surface.

The experimental non-faradic impedance spectra were fitted with computer simulated spectra using an electronic circuit shown in Fig. 5. This equivalent circuit includes the ohmic resistance of the electrolyte solution, Rs, the Warburg impedance, Zw, from the diffusion, the constant phase element, CPE, and membrane resistance, Rm. The latter three components,

Zw, CPE and Rm, represent interfacial properties of the electrode, and they are affected by the surface modification.
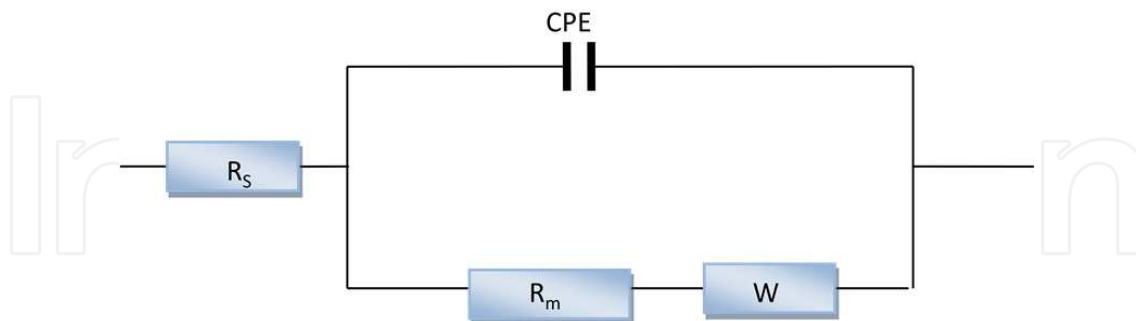
Figure 5. Equivalent circuit used to model impedance data in PBS solution.

An excellent fitting between the simulated and experimental spectra was obtained for the bare Au-electrode and the mixed monolayer-modified Au-electrode Fig. 6.A. It can be seen that the diameter of semi-circle at high frequency increases upon the stepwise formation of modifier on the electrode surface. The membrane resistance values, Rm, were extracted from the computer simulated spectra which are 2180 and 13967 Ωcm^2 for bare Au-electrode and mixed modified Au-electrode, respectively.

The values of the fractional coverage area of the mixed monolayer (θ) can be calculated from the impedance diagrams using equation 6 [33]:

$$\theta = 1 - \frac{R_m}{R_m^*} \qquad (6)$$

where R_m and R_m^* are the values of the membrane resistance derived from the impedance diagram of the bare gold electrode and mixed self-assembled monolayer, respectively. In our system the fractional coverage area was equal to 0.84. The high value of the Warburg impedance of the gold electrode with the covered SAM shows that the layer is not acting as a blocking layer but as a diffusion layer because of the low percentage of area coverage.

The experimental variations of impedance versus time show a stability in the range of 8%, which proves the mixed SAMs is quite stable. Such stability of the mixed monolayer offers us a very good basis for further construction.

Cyclic voltammetry experiments further confirmed that the mixed SAM was successfully formed on the gold surface. When the electrode surface was modified by addition of material, the electron transfer kinetics of $Fe(CN)_6^{-4/-3}$ were perturbed. As shown in Fig. 6.B, the stepwise assembly of bare gold and mixed SAMs is accompanied by a decrease in the peak to peak separation between the cathodic and anodic waves of redox probe. This shows the formation of the mixed monolayer.
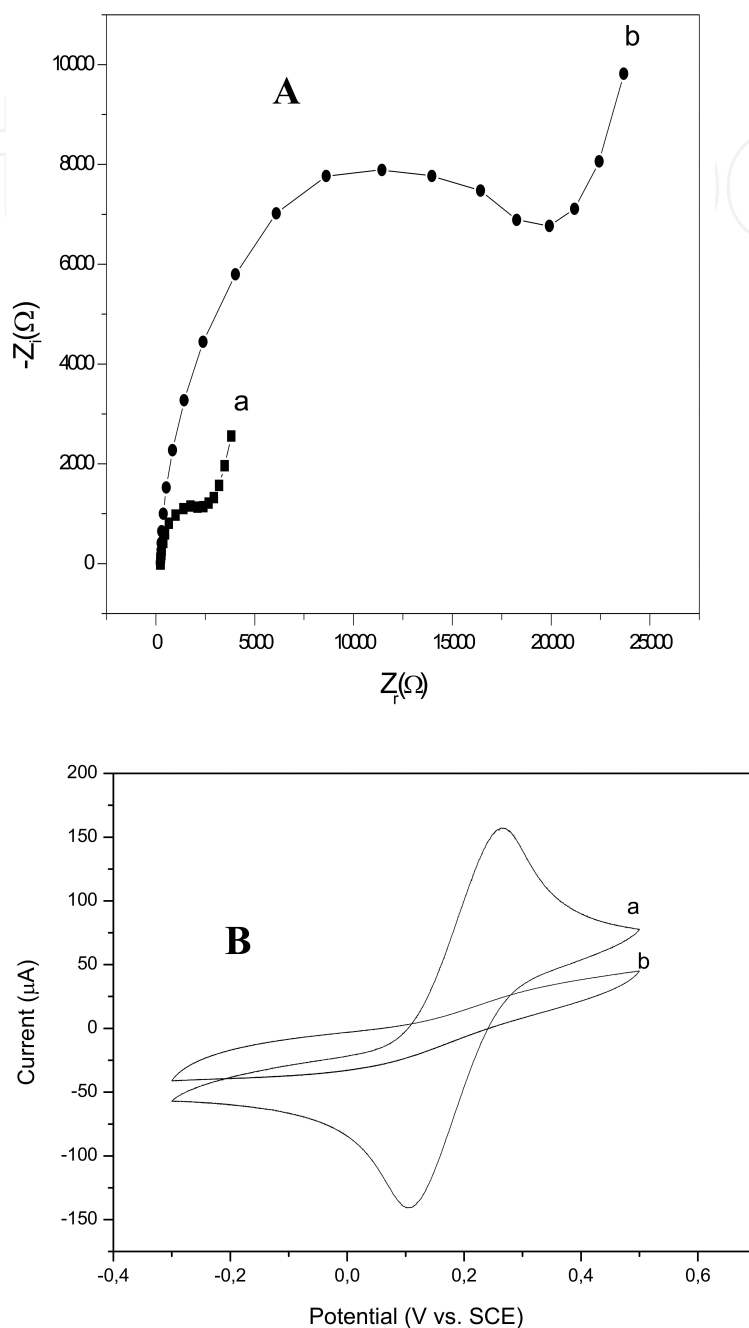
Figure 6. (A) Nyquist diagram (Zr vs.Zi) for the non faradic impedance measurements corresponding to (a) bare Au-electrode and (b) mixed self-assembled monolayer functionalized Au electrode. Symbols show the experimental data in PBS solution. Solid curves show the computer fitting of the data using the equivalent circuits shown in Fig. 5. (B) Cyclic voltammetry for bare gold and mixed SAM electrodes in 5 mM K3[Fe(CN)6]/K4[Fe(CN)6] in PBS pH 7.0.

4.1.2. Recognition properties of the self-assembled multiplayer

In order to evaluate the recognition properties of the system, in terms of sensitivity and se‐ lectivity, we exposed the gold electrode with self-assembled multilayers to various concen‐ trations of atrazine after immobilization of biotinyl-Fab fragment K47 antibody. The corresponding Nyquist plots of impedance spectra are shown in Fig.7 the semicircle diame‐ ter in Nyquist plot seems to decrease with the antigene concentration, implying that more amount of antigen was linked to the interface and the mixed SAMs change its structure with different concentration adding of antigen as the antigen was not immobilized on the entire surface and thus do not act as a blocking layer.

When the concentration of antigen was increased over 300 ng/ml, the change of impedance spectroscopy become gradually weak, showing that immobilization of the antibody on a gold electrode trends to saturation situation. So we can conclude that the self-assembled multilayer system that we developed allows distinguishing between specific immobilization of a given receptor and parasitic adsorption of the other proteins present, and thus repre‐ sents an efficient means to constitute a biosensor for detection of atrazine. Taking into ac‐ count the blank and the signal fluctuation (noise), the detection limit for the binding of atrazine on the self-assembled multilayer is 20ng/ml.

4.2. Functionalized magnetic beads

Recently, many improvements including enhanced sensitivity and reduced detection time have been made to immunosensors. These improvements are considerably attributed to the use of magnetic beads (MBs) in immunosensors. MBs allows (i) easy separation and localiza‐ tion of target proteins by an external magnet, (ii) fast immunoreactions between antigen and antibody, and (iii) low nonspecific binding by surface modification[34]. Recently, MB-based immunoassay systems are widely used in clinical laboratories, and MB-based immunoassay becomes one of standard formats in high-throughput assay. The lowest detection limit of these immunoassay system is generally in the pg/mL range. Accordingly, a more sensitive detection method based on MB is required. Recently, many electrochemical immunosensors using MB have been developed to achieve low detection limits. The high interest in electro‐ chemical immunosensors is due to their easy miniaturization and operation [35-37].

EIS correlates parameters of the system that are purely electrochemical, i.e. current/potential [38]. Nevertheless, electrochemical systems have also been studied by extending the impe‐ dance concept to measurement obtained by application of perturbations of a non-electrical character, such as temperature, magnetic field, illumination, etc., and in the measurement of the responses of the responses of non-electrical character, such as optical transmittance, mass determination via a quartz balance etc., after an electrochemical perturbation

Here, we present an ultrasensitive and promising analytical method employing an electro‐ chemical immunosensing strategy based on magnetic monolayer of magnetic particles coat‐ ed with streptavidin. This novel strategy takes advantage of easy magnetic separation and immunoreaction by MB and a high binding affinity between the biotin/ streptavidin couple.
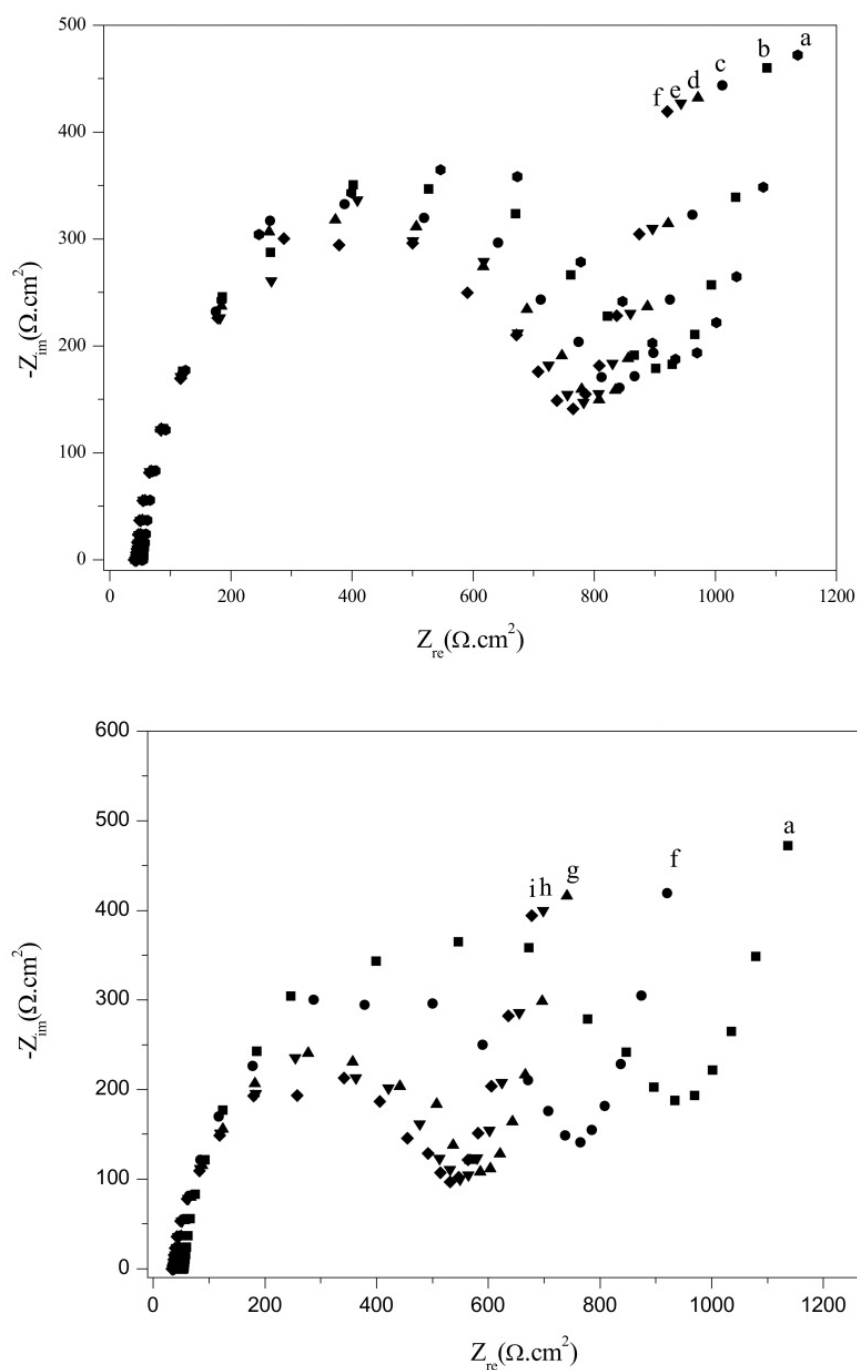
Figure 7. Complex impedance plots of antigen–antibody/neutravidin/blocking with IgG/mixed SAM/gold electrode under various concentrations of atrazine. The concentrations of atrazine (ng/ml): (a) 0; (b) 10; (c) 30; (d) 50; (e) 80; (f) 120; (g) 200; (h) 600; (i) 1100.

4.2.1. Characterization of magnetic monolayer [39]

The magnetic coated streptavidin nanoparticles that display a diameter of 200 nm and an iron oxide content of about 70%. A schematic illustration of the nanoparticle is presented in Fig. 8. After application of a 300 mT magnetic field, a layer of magnetic particles coated with streptavidin was formed on the gold electrode.

FeO$_x$

Streptavidin

Mean diameter 200nm
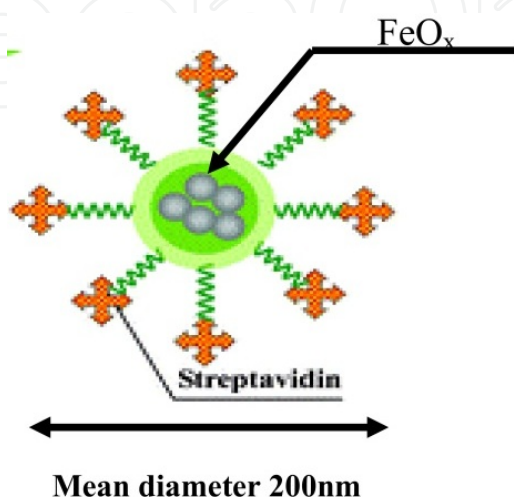
**Figure 8.** Nanoparticles structure.

The magnetic monolayer was characterized using faradaic impedance spectroscopy, cyclic voltammetry and atomic force microscopy (AFM) techniques.

Cyclic voltammetry experiments further confirmed that a magnetic monolayer was successfully formed on the gold surface. When the electrode surface was modified by addition of material, the electron transfer kinetics of $[Fe(CN)_6]^{4-/3-}$ were perturbed.

The stepwise assembly of bare gold and magnetic beads is accompanied by a decrease in the peak to peak separation between the cathodic and anodic waves of the redox probe. This result shows that the magnetic monolayer formed on gold electrode is not a real insulating layer but presents a conductivity near the gold surface.

In order to characterize the formation of the magnetic monolayer and obtain information on its architecture, AFM measurement were taken in tapping mode. Fig.9 shows an AFM image of the bare gold and of the magnetic beads layer. The image shows the formation of magnetic monolayer homogeneous and dense. The line profile measurement of the magnetic beads give diameter distribution 200 nm witch fit will with real beads dimension.

The faradic impedance spectra for bare gold electrode and the magnetic monolayer show a strong decrease in the constant phase element. It is evident such a constant phase element decrease can simply be attributed to a change in the thickness. Further, we have a decrease in electron transfer resistance. This decrease could be due to changes in surface conductivity.
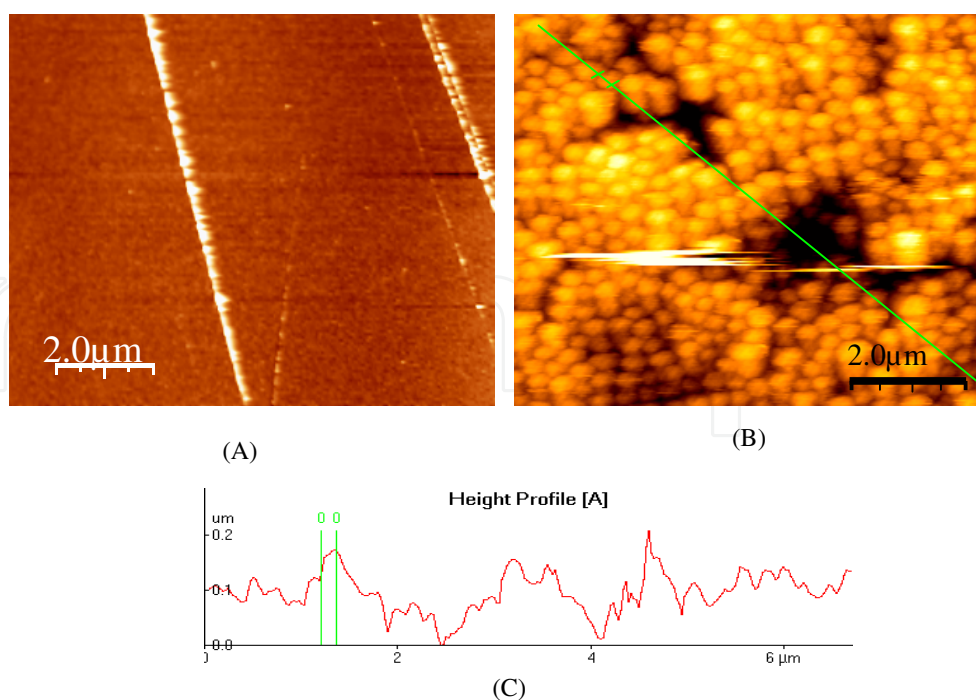
Figure 9. AFM image of (a) bare gold, (b) deposited magnetic beads on gold electrode and (c) profile measurement of magnetic beads.
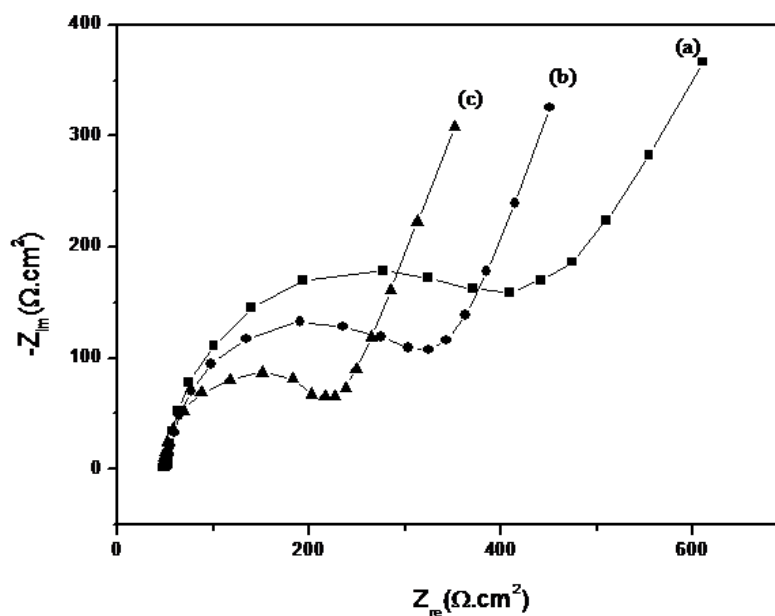

Figure 10. Nyquist diagram (Zr vs. Zi) for the non-faradaic impedance measurements corresponding to: (a) magnetic beads/Au-electrode; (b) Fab fragmentK47 antibody/magnetic beads/Au-electrode; (c) 600ng/ml Atrazine/Fab fragment K47 antibody/magnetic beads/Au-electrode. Solid curves show the computer fitting of the data. Symbols show the experimental data.

4.2.2. Atrazine detection

The antibody, biotinyl–Fab fragment K47, forms a quite stable layer onto the magnetic monolayer due to the high affinity of the biotin/streptavidin interaction. After the antibody layer formation an antigen, atrazine was injected to react with the antibody.

Complex impedance plots of the successive buildind-up of the sensing layer are shown in fig. 10. To analyze the complex impedance spectra, data were fitted with the commercially available software Zplot/Zview (Scibner Associates Inc.) to equivalent circuit:
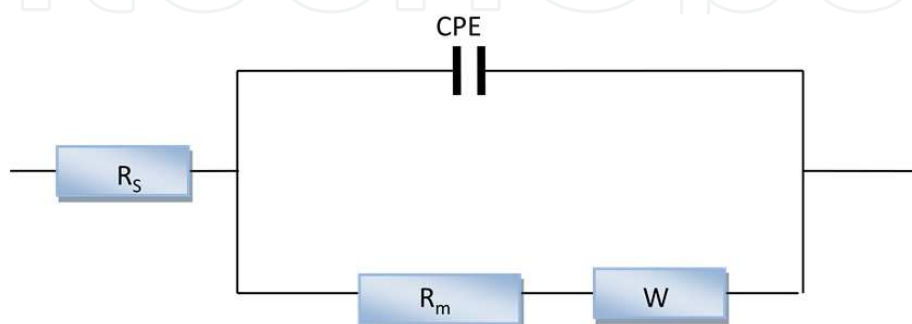
The electron transfer resistance values were 304.6 Ωcm^2, 204.5 Ωcm^2 and 188.5 Ωcm^2 for the magnetic monolayer, the antibody layer and after injection of 600 ng/ml of atrazine, respectively. The decreases of electron transfer resistance could be attributed to a reorganization of the beads as the constant phase element decreases too. The constant phase elements, Q, extracted from the computer fitting for the same steps were 17$\mu F/cm^2$,15$\mu F/cm^2$ and 14.29$\mu F/cm^2$, respectively. This decrease is due to an increase in thickness.

In order to test the specific binding of the magnetic monolayer, we exposed the substrate to various concentrations of atrazine, and Nyquist plots were recorded using EIS. A significant difference in the impedance spectra was observed with increasing receptor concentration. A linear relationship between the ΔR_{et} values and the concentration of atrazine was established in the range from 50ng/ml to 500ng/ml.

4.3. Polypyrrole–neutravidin layer

A variety of methods capable of immobilizing biologically active material onto or in close proximity of the transducer surface have been reported. The conducting polymers can be considered as effective material for immobilization of biomolecules and for transducing/ amplification of electrical signal in design of immunosensing devices [40,41]. The conjugated double bonds in the backbone of the conducting polymers allow free movement of electrons within the conjugating length, which makes them electrically conductive [42]. Till now, polypyrrole (PPy) has mostly been applied because of its high conductivity, high storage ability, good thermal and environmental stability, high redox and capacitive current and biocompatibility. Polypyrrole can be synthesized by chemical polymerization [43], photoinduced synthesis [44] and electrochemical activation by anodic current[45]. Electrochemical polymerization is the most commonly used procedure to deposit conductive polymers due

to its simplicity and rapidity. During the electrochemical oxidation process, biomolecules can be added into the monomer solution for subsequent entrapment. Typically, this polymer/biomolecule layer is developed at fixed potentials or by cyclic voltammetry. The method allows the polymeric layer to be controlled, but could also lead to the denaturation of the biologically active element during the immobilization process.

Moreover, by using this technique, thickness and morphology of deposited layer might be controlled by application of well-defined potential and known current passing through the electrochemical cell

In this approach, we present another way to immobilize biomaterials based on neutravidin entrapment during electrochemical deposition of polypyrrole. The attachment of biotinyl–Fab fragment K47 antibody through the specific biotin–neutravidin interaction was therefore done on the total volume of the polypyrrole layer.

4.3.1. Preparation of the PPy/neutravidin layer [46]

In order to obtain a semi-transparent and thin polypyrrole film, we minimize the duration of the cyclic voltammetry. The polypyrrole film with yellow color can be obtained with cyclic voltammetry between 600 and 900mV. A reproducible PPy/neutravidin thickness layer can be realized with the same method. However, the majority of proteins are not highly charged in neutral pH. We have therefore used an anionic surfactant (SDS) as a co-dopant in order to add an ionic behavior to the proteins which is very useful for the entrapment process within the biofilm [47]. The confirmation the incorporation of neutravidin inside the Polypyrrole film was studied by impedance spectroscopy. The impedance spectroscopy measurement give big change in charge transfer resistance. If large size dopant molecules such as neutravidin were incorporated into PPy film during electropolymerization, the polypyrrole layer might to have a porous structure. Therefore, we can confirm that neutravidin was inside the PPy film since the high resistance deduced from the impedance plot was generally expected to be related to the porous structure.

4.3.2. Immunoassay

After blockage of nonspecific sites close to the biofilm with Bovine serum albumin (BSA), the subsequent grafting of Fab fragment will therefore be based only on biotin–neutravidin bonding. This interaction is very rapid and the strongest known non-covalent binding with a dissociation constant of 10^{-15} M [38]. The Nyquist plot after antibody attachment had a semicircle shape which indicating a film charge-transfer resistance. It is clear that Fab fragment loading affect the dynamics of charge transfer near the electrode interface due to differences in the electroconductivity between PPy/neutravidin film and Fab immobilized surface. A non-homogenous insulating protein layer was therefore added on the biofilm after fixation of the immunoreceptor.

In order to assess the immunosensor sensitivity, different concentrations of atrazine in the range of 0.1–200ng/ml were injected on the Fab fragment modified electrode show an increase in the semicircle diameter with antigen concentration. This was related to the positive

change in the film charge transfer resistance after atrazine injection. An insulating organic layer was progressively added to the biofilm since an immunoreactions near the electrode surface was established between the Fab fragment and the antigen. This interaction might affect the thickness of the double couche at the electrode interface. Fig.11 illustrates very well the good sensitivity of our impedimetric immunosensor even with 0.1ng/ml of atrazine. However, this excellent antigen detection limit could have an important non-specific part. Thus, different concentrations of rabbit IgG (non-specific antigen) in the range of 0.1–200 ng/ml were added to the biosensor. The impedance measurements show a very little increase in the Nyquist plot diameter with respect to the atrazine detection.

Based on all these results and in order to illustrate the sensitivity and the selectivity of the immunosensor, two curves corresponding to the variation of ∆Rt (∆Rt is the change of charge transfer resistance obtained by subtracting the resistance of the immobilized biotinylated Fab fragment from the resistance of the immune complex) with atrazine and rabbit IgG concentrations were plotted (Fig. 11).
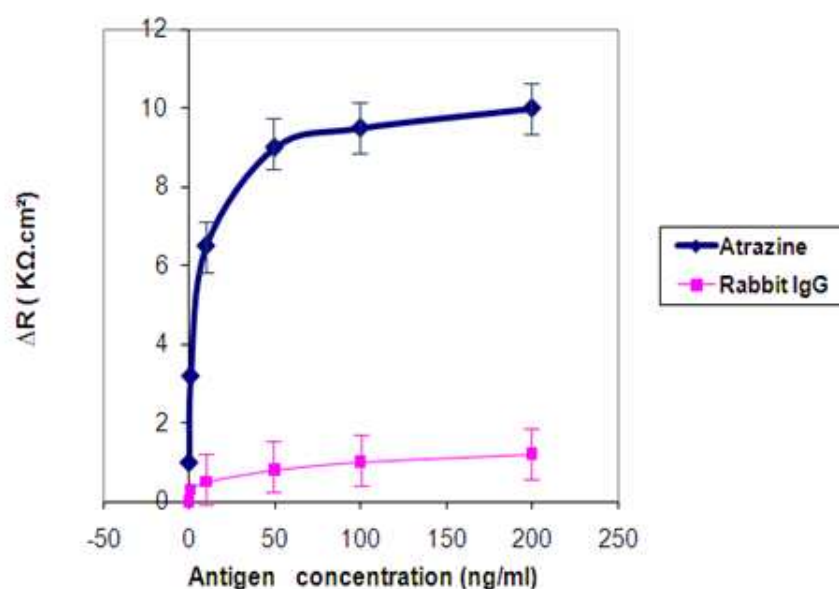
Figure 11. The variation of ∆Rt with atrazine and rabbit IgG concentrations

As can be seen in Fig. 11, the plot for the atrazine detection was almost linear and tend to reach saturation next to 200ng/ml. Whereas the response of the immunosensor to different concentrations of non-specific antigen was clearly non-significant. These results have been obtained with a good reproducibility. We are therefore sure that the above-observed impedance changes after atrazine injection were generated from the result of specific Fab fragment-antigen interaction.

4.4. Labeled magnetic nanoparticles assembly on polypyrrole film

In recent years, conducting polymers combined with metallic nanoparticles have been paid more attention due to their potential applications in microelectronics, microsystems, optical

sensors and photoelectronic chemistry. In many recent works, PPy films are found to be associated with metallic nanoparticles (NPs) [48]. The development of such nanocomposites is essentially motivated by their high analytical sensitivity in sensing applications. Different properties emerging from the nanostructuration with NPs are at the origin of the increased sensing sensitivity. The NPs size and high surface area have first the ability to facilitate direct and fast electron transfer between the nanocomposite and the transducer. Second, when compared to homogeneous bulk matrices, the high surface area of the NPs assembly also leads to nanoporosity for signal amplifications and increased sensitivity toward surface adsorption or surface reactions. Because of the same geometric properties the NPs assembly also allows minimum diffusion of the target molecule, and in the same time, miniaturization of the device. Finally it was shown that the selectivity of the sensor could been hanced by tuning the molecular interactions between the NPs and linker molecules. The improvement of the sensing properties resulting from the nanostructuration is such that various routes were proposed in order to incorporate NPs either in the PPy film or by synthesis of the metallic NPs directly on the PPy film.

We addressed this study to the preparation and characterization of a nanocomposite composed by a thin polypyrrole (PPy) film covered with an assembly of magnetic nanoparticles (NPs). The magnetic particles were immobilized on PPy films under appropriate magnetic field in order to control their organization on the PPy film and finally to improve the sensitivity of the system in potential sensing applications (Fig.12).
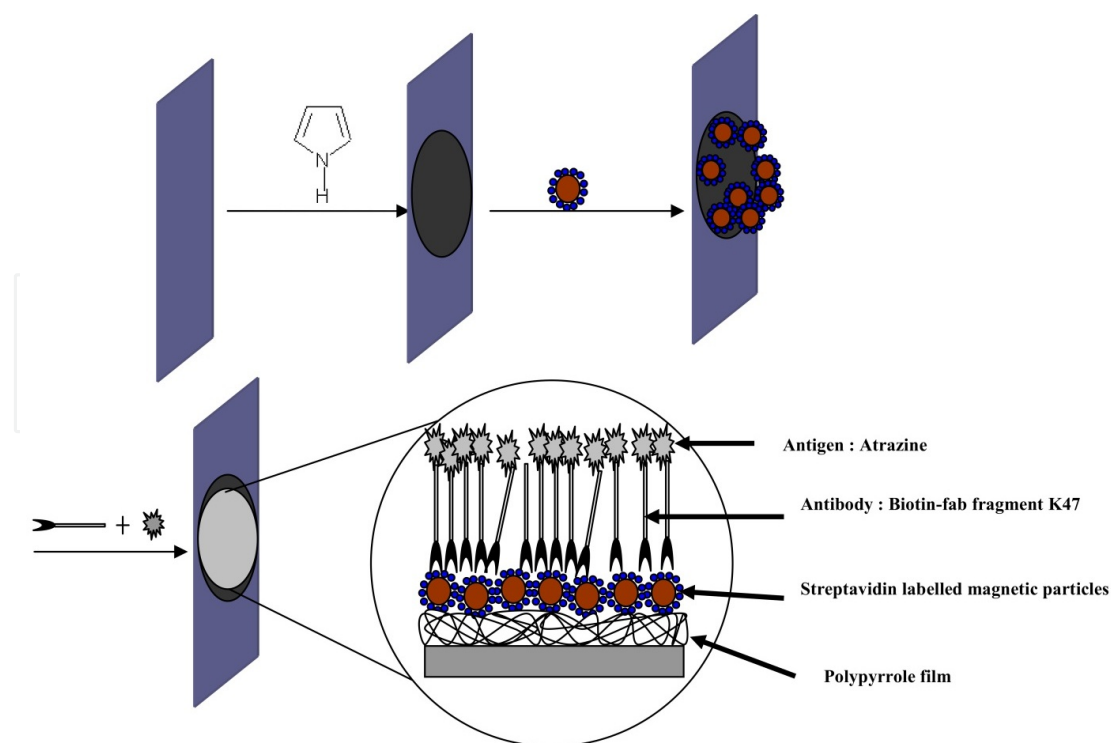

Figure 12. A schematic diagram of the immunosensor showing the stepwise immunosensor fabrication process.

4.4.1. The polypyrrole film/magnetic nanoparticles composite [49]

The atomic force microscopy images of the PPy film shown in Fig.13.A. These micrographs reveal the cauliflower morphology usually observed for electrochemically deposited PPy films which is attributed to the nodular fractal-type growth of these polymers. However, the high roughness of this surface does not allow atomic force microscopy acquisitions on large area. The NPs assembly is clearly observable with atomic force microscopy as shown in Fig. 13.B. Cracks in the NPs assembly are again present at microscopic scale. AFM observations allow us to assess for the distribution of both the PPy and the NPs on the electrode, which should provide enhanced adsorption and sensitivity in sensing application.
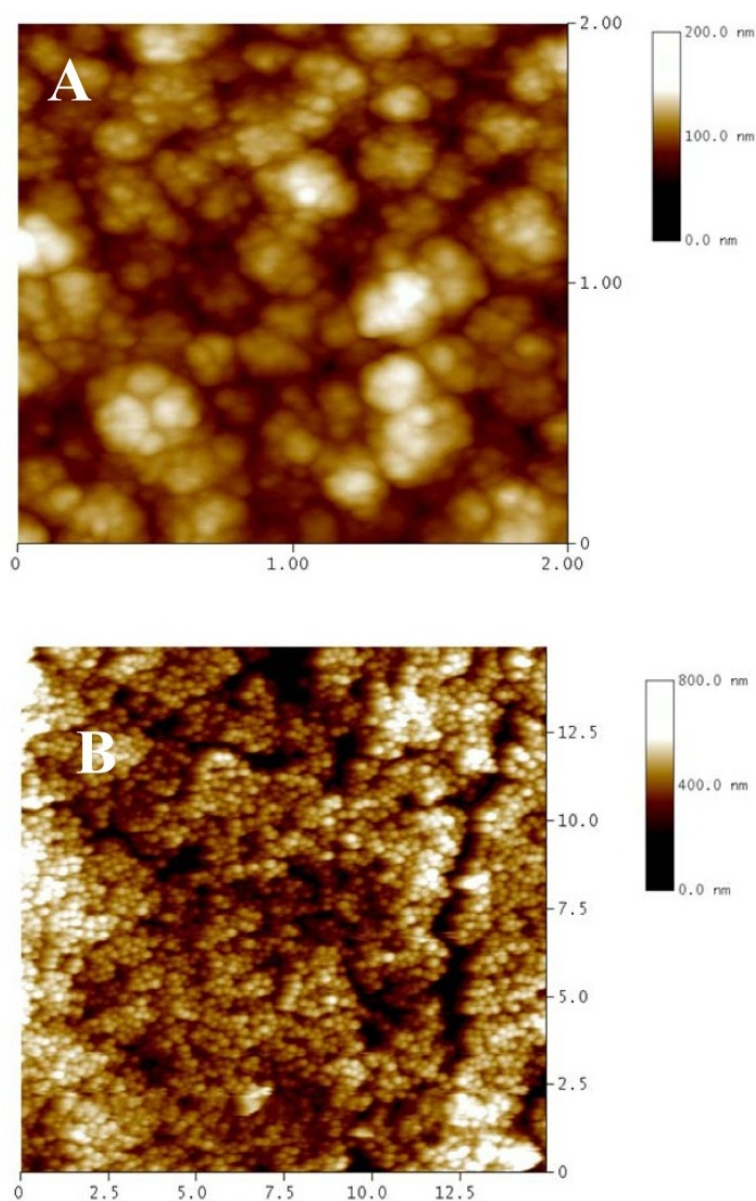
Figure 13. Top AFM images of: (A) PPy film showing the cauliflower structure of this polymer, (B) PPy film covered with an array of nanoparticles

Cyclic voltammograms of the gold electrode present a reversible phenomenon, which is the typical behaviour of gold surface with redox couple (Fig.14). The two peaks of the cathodic and anodic waves of redox probe have been obtained. After modification of the gold surface with PPy, the dc-current increases due to the conducting properties of the PPy film. After immobilization of the magnetic particles on the PPy film, the direct current decreases due to the insulating properties of the functionalized film (streptavidin) covering the particles. The same explanation applies for the decrease of the direct current after immobilization of the antibody and after the BSA blocking step.
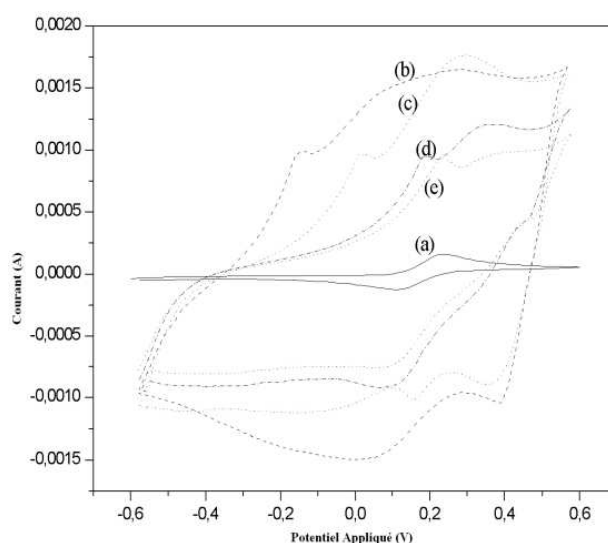
Figure 14. Cyclic voltammograms after different steps of modification: (a) bare gold electrode, (b) PPy film modified gold electrode, (c) PPy covered with streptavidin labelled magnetic particles,(d) immobilization of the antibody biotin-Fab fragment K47 and (e) BSA blocking layer.

Fig. 15 shows the impedance spectrum of a PPy film coated gold electrode (curve a) compared with streptavidin labeled magnetic particles surface (curve b), with an antibody-immobilized surface (curve c) and with BSA blocking layer (curve d).

Note that all the spectra are almost similar, containing a distorted semicircle. The diameter of the semicircle provides an estimate of the film charge transfer resistance. The resistance of the studied interface increases after the immobilization of each step. This increase is due to the decrease of the conductivity due to the insulating properties of grafted layers. This confirms the results obtained with cyclic voltammetry.

4.4.2. Biosensor application

Biotinylated Fab fragment K47 antibody was covalently bound to the particles through streptavidin/biotin linkage. This allows specific bounding of atrazine on the NPs and varia-

tion of the electrode impedance response. Atrazine–antibody interactions were monitored by impedance spectroscopy at −1200mV. The semicircle diameter in the impedance spectroscopy measurement is increasing with the atrazine concentration, implying that more amount of atrazine was linked to the interface. These results revealed that the presence of the PPy film under the NPs assembly increases over four orders of magnitude the sensitivity of the sensor as compared to only the NPs assembly, with an excellent detection limit of 5ng/ml [38].
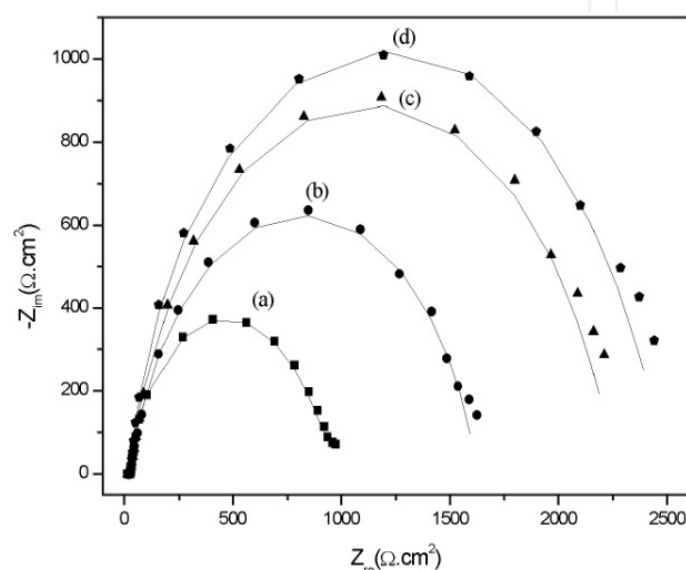
Figure 15. Nyquist diagram for the faradic impedance measurements corresponding to (a) PPy film/Au-electrode, (b) streptavidin labeled magnetic particles/PPy film/Au-electrode, (c) biotin-Fab fragment K47 antibody/streptavidin labeled magnetic particles/PPy film/Au-electrode and (d) blocked layer with BSA/biotin-Fab fragment K47 antibody/ streptavidin labeled magnetic particles/PPy film/Au-electrode. Solid curves show the computer fitting. Symbols show the experimental data.

5. Conclusion

Over the last few years, there have been an increasing number of publications concerning the application of biosensors to environmental analysis. Biosensors have been reported for the commonly used pesticides and industrial chemicals. In some cases there is a need for sensitivity and lifetime improvements as conventional techniques can outperform biosensors in these respects at present. The health and safety of workers applying pesticides or indeed any other chemical could be protected by providing them with biosensors for monitoring the levels of pesticides or chemicals in the air around them. Biosensors could contribute towards monitoring the progress of clean-up operations after environmental spillages of certain chemicals.

Author details

Saloua Helali

Address all correspondence to: salwahleli@yahoo.fr

Research and Technology Centre of Energy, Hammam Lif, Tunisia

References

[1] COM(2006) 398 final: Proposal for a Directive of the European Parliament and of the Council of 17 june, 2006 on environmental quality standards in the field of water policy and amending Directive 2000/60/EC.

[2] Nanoporous impedemetric biosensor for detection of trace atrazine from water samples: Pie Pichetsurnthorn, Krishna Vattipalli , Shalini Prasad. Biosensors and Bioelectronics, Volume 32, 2012, Pages 155-162.

[3] A direct optical immunosensors for atrazine detection: Andreas Brecht, Jacob Piehler, Gerd Lang, Günter Gauglitz: Analytica Chimica Acta, Volume 311, 1995, Pages 289-299.

[4] Separation-free electrochemical immunosensor for rapid determination of atrazine: R.W. Keay, C.J. McNeil. Biosensors and Bioelectronics, Volume 13, 1998, Pages 963-970.

[5] Effects of atrazine on periphyton under grazing pressure: Isabel Muñoz, Montserrat Real, Helena Guasch, Enrique Navarro, Sergi Sabater: Aquatic Toxicology, Volume 55, 2001, Pages 239-249.

[6] Pesticide determination in tap water and juice samples using disposable amperometric biosensors made using thick-film technology: Miquel Albareda-Sirvent, Arben Merkoçi, Salvador Alegret: Analytica Chimica Acta, Volume 442, 2001, Pages 35-44.

[7] Plant tissue electrode for the determination of atrazine: Franco Mazzei, Francesco Botrè, Giampiero Lorenti, Giovanna Simonetti, fernando Porcelli, Giancarlo Scibona, Claudio Botrè: Analytica Chimica Acta, Volume 316, 1995, Pages 79-82.

[8] Council Directive of 15 July 1980 relating to the quality of water intended for human consumption (80/778/EEC).

[9] Construction and characterization of the direct piezoelectric immunosensor for atrazine operating in solution: Clemens Steegborn & Petr Skliidalt. Biosensors & Bioelectronics Vol. 12. pp. 19-27, 1997.

[10] Immunochemical methods for environmental monitoring: Gianfranco Giraudi, Claudio Baggiani, Nuclear Medicine and Biology, Volume 21, 1994, Pages 557-572.

[11] Applications of electrochemical immunosensors to environmental monitoring: Omowunmi A. Sadik, Jeanette M. Van Emon: Biosensors and Bioelectronics, Volume 11, 1996.

[12] Biosensors for pesticide detection basedon alkaline phosphate-catalyzed chemiluminescence: Madhu S.Ayyagari, Sanjay Kamtekar Rajiv Pande, Kenneth A. Marx, Jayant Kumar, Sukant K. Tripathy, David L. Kaplan: Materials Science and Engineering: C, Volume 2, 1995, Pages 191-196

[13] Conductimetric immunosensor for atrazine detection based on antibodies labelled with gold nanoparticles: Enrique Valera, Javier Ramón-Azcón, F.-J. Sanchez, M.-P. Marco, Ángel Rodríguez: Sensors and Actuators B: Chemical, Volume 134, 2008, Pages 95-103.

[14]] Label-free impedimetric immunosensor for sensitive detection of atrazine: Rodica E. Ionescu, Chantal Gondran, Laurent Bouffier, Nicole Jaffrezic-Renault, Claude Martelet, Serge Cosnier: Electrochimica Acta, Volume 55, 2010, Pages 6228-6232.

[15] Impedimetric immunosensor for atrazine detection using interdigitated μ-electrodes (IDμE's): Enrique Valeraa, Javier Ramon-Azconb, Angel Rodrigueza, Luis M. Castanera, F.-J. Sanchezb, M.-P. Marco: Sensors and Actuators B 125 (2007) 526–537

[16] Antibodies for immunosensors: A review, Bet-told Hock, Analytica Chimica Acta 347 (1997) 177-186

[17] Immunosensors for detection of pesticide residues: Xuesong Jianga, Dongyang Li, Xia Xu, Yibin Ying, Yanbin Li, Zunzhong Ye, Jianping Wang, Biosensors and Bioelectronics 23 (2008) 1577–1587.

[18] Nanomaterial labels in electrochemical immunosensors and immunoassays: Guodong Liu, Yuehe Lin, Talanta 74 (2007) 308–317.

[19] Lewis, Lord of Newnham (1992) (chairman) commission on environmental pollution,16th report, HMSO, London.

[20] Needs for reliable analytical methods for monitoring chemical pollutants in surface water under the European Water Framework Directive. Peter Lepom, Bruce Brown, Georg Hanke, Robert Loos, Philippe Quevauviller, Jan Wollgast, Journal of chromatography A, 1216 (2009) 302-315;

[21] Semi disposable reactor biosensors for detecting carbamate pesticides in water: Siriwan Suwansa-ard, Proespichaya Kanatharana, Punnee Asawatreratanakul, Chusak Limsakul, Booncharoen Wongkittisuksa, Panote Thavarungkul, Biosensors and Bioelectronics, Volume 21, 2005, Pages 445-454.

[22] highly sensitive organophosphorous pesticide biosensors based on nanostructured films of acetylcholinesterase and CdTe quantum dots: Zhaozhu Zheng, Yunlong Zhou, Xinyu Li, Shaoqin Liu, Zhiyong Tang,Biosensors and Bioelectronics, Volume 26, 2011, Pages 3081-3085.

[23] Amperometric inhibition-based detection of organophosphorus pesticides in unary and binary mixtures employing flow-injection analysis: Ivaylo Marinov, Yavor Ivanov, Nastya Vassileva, Tzonka Godjevargova,Sensors and Actuators B: Chemical, Volume 160, 2011, Pages 1098-1105

[24] Construction and characterization of the direct piezoelectric immunosensor for atrazine operating in solution: Clemens Steegborn, Petr Skládal, Biosensors and Bioelectronics, Volume 12, 1997, Pages 19-27.

[25] Local electrochemical impedance spectroscopy: A review and some recent developments, Vicky MeiWen Huang, Shao-Ling Wu, Mark E. Orazem, Nadine Pébère, Bernard Tribollet, Vincent Vivier, Electrochimica Acta

[26] Application of electrochemical impedance spectroscopy to study the degradation of polymer-coated metals: A. Amirudin, D. Thierry, Progress in Organic Coatings 26 (1995) 1-28.

[27] Impedance spectroscopy: Over 35 years of electrochemical sensor optimization: Bobby Pejcic, Roland De Marco, Electrochimica Acta 51 (2006) 6217–6229

[28] Impedimetric immunosensors-A review: Mamas I. Prodromidis, Electrochimica Acta 55 (2010) 4227-4233

[29] Impedance spectroscopy: J.Ross Macdonal, Annals of biomedical Engineering, volume 20, 1992, pages 289-305.

[30] Comparison of Different Protein Immobilization Methods on Quartz Crystal Microbalance Surface in Flow Injection Immunoassay: Yung-Chuan Liu, Chih-Ming Wang, and Kuang-Pin Hsiung. Analytical Biochemistry 299, 130–135 (2001)

[31] Micocontact printing of proteins on mixed self-assembled monolayer J.L. Tan, J. Tien, C.S. Chen, Langmuir 18 (2002) 519.

[32] Atrazine analysis using an impedimetric immunosensor based on mixed biotinylated self-assembled monolayer: S. Hlelia,, C. Martelet, A. Abdelghani, N. Burais, N. Jaffrezic-Renault. Sensors and Actuators B 113 (2006) 711–717

[33] A correlation study between the conformation of the 1,4-dithiane SAM on gold and its performance to assess the heterogeneous electron-transfer reactions: J.R. Sousa, M.M.V. Parente, I.C.N. Diogenes, L.G.F. Lopes, P.L. Neto, M.L.A. Temperini, Al.A. Batista, I.S. Moreira, J. Electroanal. Chem. 566 (2004) 443.

[34] Ultrasensitive electrochemical immunosensing using magnetic beads and gold nanocatalysts: Thangavelu Selvaraju, Jagotamoy Das, Sang Woo Han, Haesik Yang, Biosensors and Bioelectronics 23 (2008) 932–938.

[35] Magnetic bead-based DNA detection with multi-layers quantum dots labeling for rapid detection of Escherichia coli O157:H7, Yi-Ju Liua, Da-Jeng Yao, Hwan-You Chang, Chien-Ming Liu, Chih Chen, Biosensors and Bioelectronics Volume 24, 2008, Pages 558-565.

[36] Controlled torque on superparamagnetic beads for functional biosensors: X.J.A. Janssen, A.J. Schellekens, K. van Ommering, L.J. van IJzendoorn, M.W.J. Prins, Biosensors and Bioelectronics, Volume 24, Issue 7, 15 March 2009, Pages 1937-1941.

[37] Monitoring the growth and drug susceptibility of individual bacteria using asynchronous magnetic bead rotation sensors: Paivo Kinnunen, Irene Sinn, Brandon H. McNaughton, Duane W. Newton, Mark A. Burns, Raoul Kopelman, Biosensors and Bioelectronics, Volume 26, 2011, Pages 2751-2755.

[38] An impedimetric DNA sensor based on functionalized magnetic nanoparticlesfor HIV and HBV detection: Walid Mohamed Hassen, Carole Chaix, Adnane Abdelghani, François Bessueille, Didier Leonard, Nicole Jaffrezic-Renault, Sensors and Actuators B: Chemical, Volume 134, 2008, Pages 755-760.

[39] A disposable immunomagnetic electrochemical sensor based on functionalised magnetic beads on gold surface for the detection of atrazine: Saloua Helali, Claude Marteleta, Adnane Abdelghani, Mhamed Ali Maaref, Nicole Jaffrezic-Renault. Electrochimica Acta 51 (2006) 5182–5186.

[40] Stable enzyme biosensors based on chemically synthesized Au–polypyrrole nanocomposites: John Njagi, Silvana Andreescu Biosensors and Bioelectronics 23 (2007) 168–175

[41] Polypyrrole based amperometric glucose biosensors: Minni Singh, Pavan Kumar Kathuroju, Nagaraju Jampana, Sensors and Actuators B: Chemical, Volume 143, 2009, Pages 430-443.

[42] Molecular electronics of conducting polymers: S. Roth, G. Mahler, Y. Shen, F. Coter, Synth. Met. 28 (1989) 815–822.

[43] Chemical synthesis and characterization of polypyrrole coated on porous membranes and its electrochemical stability: H. S. Lee, J. Hong, Synth. Met. 113 (2000) 115–119.

[44] Conducting polymer films by UV photo processing : Q.Fang, D.G.Chetwynd, J.W.Garden, Sens. Actuators A 99 (2002) 74–77.

[45] Polypyrrole, a new possibility for covalent binding of oxido reductases to electrode surfaces as a base for stable biosensors: W. Schuhmann, R. Lammert, B. Uhe, H.L. Schmid, Sens. Actuators B 1 (1990) 537–541.

[46] Polypyrrole–neutravidin layer for impedimetric biosensor: Chiheb Esseghaier, Saloua Helali, Heikel Ben Fredj, Asma Tlili, Adnane Abdelghani, Sensors and Actuators B 131 (2008) 584–589

[47] Synthesis and characterization of high molecular weight, highly soluble polypyrrole in organic solvents, E.J.Oh, K.S.Jang, Synth. Met. 119 (2001) 109–110

[48] Conducting Polymer Nanocomposites: R. Gangopadhyay, A. De, Chem. Mater. 12 (2000) 608.

[49] Labeled magnetic nanoparticles assembly on polypyrrole film for biosensor applications: H. Ben Fredj, S. Helali, C. Esseghaier, L. Vonna, L. Vidal, A. Abdelghani. Talanta 75 (2008) 740–747